Unusual behavior of Cooper minima of *ns* subshells in high-*Z* atoms

S. Baral,[1] S. Saha,[1,2] K. A. Dubey,[1] J. Jose,[1] P. C. Deshmukh,[3,4] A. K. Razavi,[5] and S. T. Manson[5]

[1]*Department of Physics, Indian Institute of Technology Patna, Bihta 801103, Bihar, India*
[2]*Department of Physics, Ohio State University, Columbus, Ohio 43210, USA*
[3]*Department of Physics and CAMOST, Indian Institute of Technology Tirupati, Tirupati 517506, India*
[4]*Department of Physics, Dayananda Sagar University, Bengaluru 560114, India*
[5]*Department of Physics and Astronomy, Georgia State University, Atlanta, Georgia 30303, USA*

(Received 2 February 2022; accepted 7 June 2022; published 23 June 2022)

A study of Cooper minima (CM) arising from the photoionization of 6*s*, 5*s*, and 4*s* subshells of high-*Z* atoms has been performed using Dirac-Fock (DF), two-channel relativistic-random-phase approximation (RRPA), and fully coupled RRPA. The results show huge splittings between $ns \rightarrow \varepsilon p_{3/2}$ and ns $\rightarrow \varepsilon p_{1/2}$ CM which increase with *Z* owing primarily to the relativistic interactions (spin orbit) that are attractive for the $\varepsilon p_{1/2}$ final state but repulsive for the corresponding $\varepsilon p_{3/2}$. In addition, it was found that correlation in the form of interchannel coupling (essentially configuration interaction in the final continuum states) plays a huge role in determining the location of the CM. For 6*s* photoionization, the $6s \rightarrow \varepsilon p_{3/2}$ and $6s \rightarrow \varepsilon p_{1/2}$ CM behave completely different as a function of *Z*. It was also found that for 5*s* and 4*s* photoionization, the CM move below the threshold, with increasing *Z*, and, at high enough *Z*, the $5s \rightarrow \varepsilon p_{3/2}$ and $4s \rightarrow \varepsilon p_{3/2}$ CM re-emerge into the continuum. The calculations have been carried out for the *ns* subshells of Hg ($Z = 80$), Rn ($Z = 86$), Ra ($Z = 88$), No ($Z = 102$), Cn ($Z = 112$), and Og ($Z = 118$).

DOI: 10.1103/PhysRevA.105.062819

I. INTRODUCTION

A Cooper minimum (CM) in dipole photoionization [1,2] refers to a zero (or near zero) in the transition matrix element, which can lead to a minimum in the cross section and notable characteristics in the angular distribution asymmetry parameter β [3]. These minima were discovered experimentally almost a century ago [4–6], and they arise due to the cancellation of the positive and negative parts in the dipole matrix element, which is expressible as the overlap integral of the initial and final state wave functions of the atoms [7,8]. The CM are ubiquitous in the photoionization of outer and near-outer subshells of ground states of atoms and molecules whose radial functions have at least one node and are found only in $l \rightarrow l + 1$ dipole photoionization channels [9]. Owing to this fact, the photoionization cross sections of atomic subshells having nodeless radial wave functions have a different spectral shape than subshells whose radial wave functions have nodes [10]. Since the CM are extremely sensitive to interactions within the initial discrete and final continuum states of the photoionization process, such as relativistic and correlation effects, their study serves as a most stringent test of theoretical investigations.

Considering the importance of the CM in photoionization studies, systematic surveys of the evolution of CM in the dipole matrix element as a function of atomic number *Z* have been performed, in both relativistic and nonrelativistic studies [9,11,12]. The nonrelativistic studies have shown that a CM is exhibited in the continuum energies at the atomic number *Z*, where a noded subshell first appears in the ground state. With increasing *Z*, the CM moves out to higher photoelectron energy and then back down, and moves into the discrete region with further increase in *Z* [9]. For example, the locus of $ns \rightarrow \varepsilon p$ CM follows this pattern for 3*s* to 6*s* atomic subshells. On the other hand, the introduction of the relativistic effects leads to quite different dynamics of the CM. First of all, the relativistic interactions split CM [13] so that, for example, for photoionization of an *ns* subshell we have $ns \rightarrow \varepsilon p_{3/2}$ and $ns \rightarrow \varepsilon p_{1/2}$ CM at different energies, and the energy difference increases with increasing *Z*. In addition, for high *Z*, earlier work [11,12] showed that the locus of $6s \rightarrow \varepsilon p_{3/2}$ and $6s \rightarrow \varepsilon p_{1/2}$ CM was very different as a function of *Z*; at the single-particle level of calculation, the $6s \rightarrow \varepsilon p_{1/2}$ CM moves below threshold around $Z = 86$, while the $6s \rightarrow \varepsilon p_{3/2}$ trajectory is still moving to higher photoelectron energy at $Z = 100$, the highest *Z* examined earlier. Since the known atoms of the periodic table have been extended to Og, $Z = 118$ and studies of the atomic properties are extant (see [14–17] and references therein), in the present work, we look at still higher *Z*, up to $Z = 118$, to determine if the $6s \rightarrow \varepsilon p_{3/2}$ trajectory turns around, as it does for nonrelativistic calculations at lower *Z*, or if there is new phenomenology at high *Z*. Furthermore, we extend the calculations to the inner subshells, 4*s* and 5*s*, to enquire how relativistic effects might affect the CM in these cases at the higher $Z's$.

Aside from the interest in the CM as a fundamental property of the photoabsorption process and their utility as extremely sensitive tests of theory, these CM have a very significant effect upon the spectral distribution of oscillator strength, i.e., photoionization, and other photoionization

parameters, particularly the dipole photoelectron angular distribution parameter β. This is particularly true for ns states where, in a nonrelativisitic formulation, $\beta = 2$ and is independent of energy [3]. From a physical point of view, there can be no energy dependence since there is only a single $ns \rightarrow \varepsilon p$ continuum wave in the photoionization process, so there is nothing to interfere with. In a relativistic formulation, however, there are the $ns \rightarrow \varepsilon p_{1/2}$ and $ns \rightarrow \varepsilon p_{3/2}$ continuum waves, which can interfere. The difference between them, in general, is negligible, so that β usually takes the value of 2 and is essentially energy independent. However, the relativistic splitting in the energy region between the Cooper minima in the $ns \rightarrow \varepsilon p_{1/2}$ and $ns \rightarrow \varepsilon p_{3/2}$ channels means that the respective continuum waves can be very different in this region, thereby causing significant shifts in the values of β along with strong energy dependence of it in this region. Thus, understanding the positions of the Cooper minima for ns states is an important step in understanding the photoelectron angular distributions.

To accomplish these objectives, two relativistic techniques, Dirac-Fock (DF) [18] and the relativistic random-phase approximation (RRPA) [19], are employed. The systematic evolution of the CM in the $6s \rightarrow \varepsilon p_{1/2}$ and $6s \rightarrow \varepsilon p_{3/2}$ photoionization channels as a function of Z is tested for Hg ($Z = 80$), Rn ($Z = 86$), Ra ($Z = 88$), No ($Z = 102$), Cn ($Z = 112$), and Og ($Z = 118$). In addition, we examine the physics behind the sharp differences between the dynamics of the CM in the two spin-orbit split channels, $6s \rightarrow \varepsilon p_{1/2}$ and $6s \rightarrow \varepsilon p_{3/2}$, and also scrutinize the CM in $4s$ and $5s$ photoionization channels. In Sec. II, we briefly review the methodology employed and the results are discussed in Sec. III.

II. THEORY

The photoionization cross section $\sigma_{\rm n}\kappa$ for a dipole transition from an atomic subshell designated by $n\kappa$ is (in atomic units) [19]

$$\sigma_{n\kappa} = \frac{4\pi^2\alpha}{3}\,\omega\,(|D_{j\rightarrow j+1}|^2 + |D_{j\rightarrow j}|^2 + |D_{j\rightarrow j-1}|^2), \quad (1)$$

where α is the fine-structure constant, ω is the photon energy and $D_{j\rightarrow\bar{j}}$ is the dipole transition matrix element. The present work employs two relativistic techniques to calculate the $D_{j\rightarrow\bar{j}}$: (1) the correlated RRPA and (2) the single-channel DF methodology. Although the DF technique includes the relativistic effects, the correlation effects are not accounted for. Therefore, to spotlight the effects of correlation, and to test the accuracy of the results obtained in the DF approximation, the sophisticated RRPA results are also calculated. This is of importance because the RRPA technique can only be applied to systems with closed subshells, while DF can be applied to both open- and closed-subshell atoms. Thus, the comparisons presented herein highlight the accuracy of the DF calculations.

The single particle matrix element for a photoionization transition indicated by $j \rightarrow \bar{j}$ in the dipole approximation is given by [20]

$$D_{j\rightarrow\bar{j}} = C(j,\bar{j})\int_0^\infty dr\, r[S_{\bar{j}}G_j + T_{\bar{j}}F_j], \quad (2)$$

TABLE I. Thresholds of $6s$, $5s$, and $4s$ subshells (in a.u.) of atoms considered.

Atom	Threshold energy (in a.u.)		
	$6s$	$5s$	$4s$
Hg ($Z = 80$)	0.33	5.10	30.64
Rn ($Z = 86$)	1.07	8.40	41.31
Ra ($Z = 88$)	1.62	10.00	45.68
No ($Z = 102$)	2.80	18.80	78.62
Cn ($Z = 112$)	5.68	30.04	113.41
Og ($Z = 118$)	8.98	39.86	140.89

where $S_{\bar{j}}$ and $T_{\bar{j}}$ are the radial large and small components of the continuum orbital, G_j and F_j are the large and small components of the unperturbed initial state orbital, and $C(j,\bar{j})$ is the angular coefficient; for an $ns \rightarrow \varepsilon p_{3/2}$ channel, the value of $C(j,\bar{j})$ is $(-\sqrt{4/3})$ while for an $ns \rightarrow \varepsilon p_{1/2}$ channel it is $(-\sqrt{2/3})$. Since the relativistic dipole photoionizing transitions from ns subshells are the focus of the work, we adopt the following representations for the specific transition matrix element: $D_{j\rightarrow\bar{j}}$,

$$D_{ns\rightarrow\varepsilon p_{3/2}} = -\sqrt{(4/3)}\,R_p, \quad (3)$$

$$D_{ns\rightarrow\varepsilon p_{1/2}} = -\sqrt{(2/3)}\,R_{\bar{p}}, \quad (4)$$

where R_j represents the radial dipole matrix element integral defined in Eq. (2). In the above equation, for simplicity, $p_{1/2}$ is labeled as $\bar{p}$ and $p_{3/2}$ as p. The ground state wave functions G_j and F_j of closed-shell atoms are obtained by solving the DF equations using the GRASP92 suite of codes [21]. Presented in Table I are the threshold energies (in a.u.) of $6s$, $5s$, and $4s$ subshells of all atoms we considered.

In the DF case, the continuum orbital wave functions $S_{\bar{j}}$ and $T_{\bar{j}}$ are obtained by solving the DF equation for continuum energies in the field of ionic residue, using the ELESEPA code [22]. Equation (2) is then employed to obtain the single-channel (DF) dipole matrix element. Note that the exchange interaction is accounted for in this single-channel treatment, but not correlation effects.

To account for the initial and the final state correlation effects in the photoionization process, the RRPA is employed [19]. The dipole matrix elements in the RRPA are obtained by solving the coupled RRPA equations [19,20]. In the RRPA, the effective matrix element $D^e_{j\rightarrow\bar{j}}$ includes correlation effects. Specifically, two-particle two-hole admixtures are included to represent the initial states (essentially a configuration interaction wave function) and interchannel coupling (essentially configuration interaction in the continuum) is included in the final state. The RRPA also allows the possibility of truncation, which amounts to selective coupling or decoupling of the final-state photoionization channels. To contrast the dynamics of CM as a function of Z, the $D^e_{j\rightarrow\bar{j}}$ and the $D_{j\rightarrow\bar{j}}$ are computed using both the RRPA including the coupling of all important photoionization channels and the DF methodologies respectively. Various truncated RRPA calculations are also performed to allow us to pinpoint the

specific interchannel coupling(s) that are important in each case. Photoionization cross sections (and, thus Cooper minima) at a given energy can be strongly affected through interchannel coupling by all open channels at that energy, particularly those open channels with large photoionization cross section. These cross sections will not be significantly affected by photoionization channels whose threshold are at much higher energy. This is the guiding factor in deciding the specific channels that need to be coupled in the full RRPA calculations.

It is of importance to emphasize that, while RRPA includes significant correlations, as mentioned above, it does have some limitations as well. A full RRPA calculation includes interchannel coupling among all final-state single-excitation channels of the photoionization process, i.e., final states where only a single electron is promoted from the initial state to an excited (discrete or continuum) orbital. It does not include multiple excitations such as photoionization plus excitation, i.e., photoionization leaving the atomic ion in an excited state. The omission of these multiple excitation channels should not be of huge importance for the present study since their cross sections tend to be quite small compared to the single-excitation photoionization channels that are included.

III. RESULTS AND DISCUSSION

The low-Z behavior of atomic ground state ns Cooper minima (CM), where relativistic effects are unimportant, has been studied as a function of Z in detail [11,12]. At the Z, where a given ns ($n \geqslant 3$) electron is included in the ground state, the photoionization cross section exhibits a CM quite close to the threshold. As Z increases, the CM moves to higher photoelectron energy. This occurs because, with increasing Z, the very diffuse ns wave function moves closer to the nucleus, since it sees a larger effective Z, but the continuum εp wave function, which also experiences a larger effective Z, moves in much more slowly owing to the p-wave angular momentum barrier. Thus, it requires more energy to pull the εp wave function in to the point of the CM. With further increase of Z, the trend is reversed; the locus of the dipole minimum reaches a maximum photoelectron energy and moves to lower energies, eventually moving below threshold into the discrete region. This occurs because Z becomes large enough that the εp begins to overcome the centrifugal barrier and the effective Z seen by the εp increases (percentagewise) much more rapidly than the ns, which is closer to the nucleus and sees a larger charge. As a result, the CM moves to lower photoelectron energy. Also, note that, nonrelativistically, as Z gets very large, we approach hydrogenic behavior and it is known that hydrogenic systems do not exhibit CM. And, at low Z, since relativistic interactions are small, this is the behavior for both $ns \rightarrow \varepsilon p_{1/2}$ and the $ns \rightarrow \varepsilon p_{3/2}$ photoionizing transitions.

It has been seen, however, that at high Z, owing to spin-orbit effects, the phenomenology can be different from what was seen at low Z [11,12]. In addition, it was noted that the nonrelativistic $ns \rightarrow \varepsilon p$ CM were split by spin-orbit forces so that the CM in both $ns \rightarrow \varepsilon p_{1/2}$ and the $ns \rightarrow \varepsilon p_{3/2}$ channels occur at different energies [13]. More recently, studies of the photoionization of superheavy elements [15,16] have indicated that these differences with the low-Z CM phenomenology are further increased with Z as high as $Z = 118$. Thus, since the spin-orbit force is attractive for $\varepsilon p_{1/2}$ and repulsive for $\varepsilon p_{3/2}$, it is evident that the $ns \rightarrow \varepsilon p_{1/2}$ and the $ns \rightarrow \varepsilon p_{3/2}$ CM might be strongly affected at high Z since the spin-orbit force scales as Z^4 [23]. This would tend to move the $ns \rightarrow \varepsilon p_{1/2}$ CM to lower energies, compared to the nonrelativistic position, and the $ns \rightarrow \varepsilon p_{3/2}$ CM to higher energies; this is exactly what has been predicted at high Z using single-particle methods, i.e., calculations that do not include many-body correlations [11,12]. However, correlation can be quite important in the location of a CM, especially the correlation in the form of interchannel coupling in the final continuum state of the photoionization process. This is because when a channel with a small cross section (like a channel with a CM) is degenerate with a channel with a large cross section, the mixing with the channel with the large cross section can alter the small cross section considerably [24,25]. As an example, at the Hartree-Fock level, the Xe $5s$ photoionization cross section does not have a CM [26], but upon inclusion of interchannel coupling using the RRPA methodology, a CM appears well into the continuum and agrees well with experiment [27]. With this background of the nature of relativistic (spin-orbit) and interchannel coupling effects, we proceed to the results of our calculations.

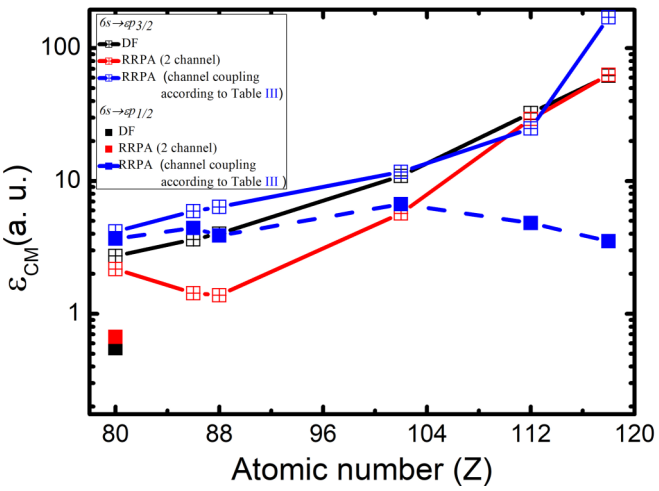

FIG. 1. Locus of $6s$ Cooper minimum locations in photoelectron energy (a. u.) on a log scale.

To begin with, the photoionization of the $6s$ subshell is considered. For Hg ($Z = 80$) with structure [Xe]$4f^{14}5d^{10}6s^2$, Table II gives the location of the $6s \rightarrow \varepsilon p_{3/2}$ CM calculated using RRPA with the 21 relativistic single-excitation channels from $6s$, $5d$, $5p$, $5s$, and $4f$ subshells, listed in Table III, to be at a photoelectron energy of 4.17 a.u., which is more than 100 eV above threshold; the results are also shown in graphical form in Fig. 1. Although many photoionization channels are omitted, they are far away in energy and have virtually no effect on the location of this CM; this is also substantiated by the fact that length and velocity results are essentially the same. We thus refer to this as *full coupling*. Also shown in Table II and Fig. 1 is the two-channel result which finds the $6s \rightarrow \varepsilon p_{3/2}$ CM at 2.17 a.u. Both the two-channel and 21-channel results have the same initial state correlation and *intrachannel* coupling (coupling between $6s \rightarrow \varepsilon p_{3/2}$ and

TABLE II. Positions of CM in 6*s* subshells in RRPA and DF in photoelectron energy (a.u.).

Atom	Photoelectron energy (a.u.) of the $6s \rightarrow \varepsilon p_{3/2}$ CM			Photoelectron energy (a.u.) of the $6s \rightarrow \varepsilon p_{1/2}$ CM		
	DF	RRPA (two channel)	RRPA (full coupling as given in Table III)	DF	RRPA (two channel)	RRPA (full coupling as given in Table III)
Hg ($Z = 80$)	2.73	2.17	4.17	0.55	0.67	3.67
Rn ($Z = 86$)	3.63	1.43	5.93			4.43
Ra ($Z = 88$)	4.01	1.38	6.38			3.88
No ($Z = 102$)	10.91	5.70	11.70			6.70
Cn($Z = 112$)	32.53	29.32	24.82			4.82
Og ($Z = 118$)	62.12	63.02	171.02			3.52

$6s \rightarrow \varepsilon p_{1/2}$ channels); thus, the difference is the result of correlation in the form of interchannel coupling which moves the $6s \rightarrow \varepsilon p_{3/2}$ CM to higher energy by 2 a.u. By performing some truncated RRPA calculations (not shown) it was found that interchannel coupling with the $5d \rightarrow \varepsilon f$ photoionization channels is the primary correlation causing the increase in the CM energy of the fully coupled RRPA result compared to the location of the two-channel RRPA CM.

The DF result for the location of the $6s \rightarrow \varepsilon p_{3/2}$ CM, from Table II and Fig. 1, is at 2.73 a.u., which gives some idea of the importance of the initial state correlations and intrachannel coupling in this case. It is also of interest to note that the nonrelativistic single-particle $6s \rightarrow \varepsilon p$ CM lies at 0.23 a.u. [9]. The fact that the nonrelativistic CM occurs at a much lower photoelectron energy highlights the role of the spin-orbit interaction in moving the continuum wave function further from the nucleus, thereby requiring more energy to move it in to overlap with the discrete wave function to result in a CM. It is, thus, evident that both relativistic effects (particularly the spin-orbit interaction) and correlation in the form of interchannel coupling are the principal determinants of the location of the $6s \rightarrow \varepsilon p_{3/2}$ CM in Hg.

Moving up in Z to Rn ($Z = 86$) with structure $[\mathrm{Xe}]4f^{14}5d^{10}6s^26p^6$, a similar story emerges. The RRPA CM with full coupling, including 26 relativistic channels, is at 5.93 a.u.; an increase over the Hg result is owing to the increase in magnitude of the repulsive spin-orbit force in the final state of the $6s \rightarrow \varepsilon p_{3/2}$ transition. Truncated RRPA calculations (not shown) indicate that coupling with $6p$ and $5d$ channels is the most important for this case. The two-channel RRPA, however, moves the CM to 1.43 a.u., a somewhat lower energy than in the Hg case. This indicates that the initial state and intrachannel coupling correlation have significant effect on the CM. The photoelectron energy of the DF CM is 3.63 a.u., an increase over the Hg result which is simply a result of the increased spin-orbit repulsion on the $\varepsilon p_{3/2}$ continuum

TABLE III. Channels coupled for the most correlated (full coupling) RRPA calculations.

Atom	Channels coupled	
Hg ($Z = 80$)	21 channels:	
		$5p_{3/2} \rightarrow \varepsilon d_{5/2}, \varepsilon d_{3/2}, \varepsilon s_{1/2}$
	$6s_{1/2} \rightarrow \varepsilon p_{3/2}, \varepsilon p_{1/2}$	$5p_{1/2} \rightarrow \varepsilon d_{3/2}, \varepsilon s_{1/2}$
	$5d_{5/2} \rightarrow \varepsilon f_{7/2}, \varepsilon f_{5/2}, \varepsilon p_{3/2}$	$5s_{1/2} \rightarrow \varepsilon p_{3/2}, \varepsilon p_{1/2}$
	$5d_{3/2} \rightarrow \varepsilon f_{5/2}, \varepsilon p_{3/2}, \varepsilon p_{1/2}$	$4f_{7/2} \rightarrow \varepsilon g_{9/2}, \varepsilon g_{7/2}, \varepsilon d_{5/2}$
		$4f_{5/2} \rightarrow \varepsilon g_{7/2}, \varepsilon d_{5/2}, \varepsilon d_{3/2}$
Rn ($Z = 86$)	26 channels:	
	21 channels listed for Hg+	$6p_{3/2} \rightarrow \varepsilon d_{5/2}, \varepsilon d_{3/2}, \varepsilon s_{1/2}$
		$6p_{1/2} \rightarrow \varepsilon d_{3/2}, \varepsilon s_{1/2}$
Ra ($Z = 88$)	28 channels:	
	26 channels listed for Rn+	$7s_{1/2} \rightarrow \varepsilon p_{3/2}, \varepsilon p_{1/2}$
No ($Z = 102$)	34 channels:	
	28 channels listed for Ra+	$5f_{7/2} \rightarrow \varepsilon g_{9/2}, \varepsilon g_{7/2}, \varepsilon d_{5/2}$
		$5f_{5/2} \rightarrow \varepsilon g_{7/2}, \varepsilon d_{5/2}, \varepsilon d_{3/2}$
Cn ($Z = 112$)	46 channels:	
	34 channels listed for No+	$6d_{5/2} \rightarrow \varepsilon f_{7/2}, \varepsilon f_{5/2}, \varepsilon p_{3/2}$
		$6d_{3/2} \rightarrow \varepsilon f_{5/2}, \varepsilon p_{3/2}, \varepsilon p_{1/2}$
		$4d_{5/2} \rightarrow \varepsilon f_{7/2}, \varepsilon f_{5/2}, \varepsilon p_{3/2}$
		$4d_{3/2} \rightarrow \varepsilon f_{5/2}, \varepsilon p_{3/2}, \varepsilon p_{1/2}$
Og ($Z = 118$)	56 channels:	
	46 channels listed for Cn+	$7p_{3/2} \rightarrow \varepsilon d_{5/2}, \varepsilon d_{3/2}, \varepsilon s_{1/2}$
		$7p_{1/2} \rightarrow \varepsilon d_{3/2}, \varepsilon s_{1/2}$
		$4p_{3/2} \rightarrow \varepsilon d_{5/2}, \varepsilon d_{3/2}, \varepsilon s_{1/2}$
		$4p_{1/2} \rightarrow \varepsilon d_{3/2}, \varepsilon s_{1/2}$

wave function. The corresponding nonrelativistic CM in Rn is at about 0.04 a.u., a decrease in photoelectron energy from Hg, as opposed to the increase in the relativistic case. In other words, completely different behavior of the $6s$ CM emerges when relativistic interactions are considered.

Increasing Z by 2 to Ra ($Z = 88$) with structure $[\mathrm{Xe}]4f^{14}5d^{10}6s^26p^67s^2$ adds only a $7s$ subshell whose cross section is rather small. Thus, one expects virtually the same story here as for Rn, and that is exactly what is seen in Table II. Of interest here is the fact that the nonrelativistic CM, which was just marginally above threshold for Rn has now moved below threshold [9], again highlighting the stark differences between relativistic and nonrelativistic behavior; it is also noteworthy that the nonrelativistic CM remains below threshold for all higher Z atoms [9].

Looking now at No ($Z = 102$), a closed $5f$ subshell is added so that the ground state structure becomes $[\mathrm{Xe}]4f^{14}5d^{10}5f^{14}6s^26p^67s^2$. In the fully coupled RRPA, the CM has been moved out to a photoelectron energy of 11.70 a.u., while the two-channel CM is at 5.70 a.u. Thus, in this case, the interchannel coupling, mostly with the $5f$ channels (which dominate the total cross section [15]), moves the CM to higher energy by more than 5 a.u. (or more than 136 eV). The DF result is at 10.91 a.u., showing the steady increase with Z that is due to the repulsive spin-orbit force, which increases with Z, and which is quite close to the fully coupled result. These results show that correlation can engender considerable alteration in the position of the CM, as seen by a comparison of the fully coupled and two-channel results, along with the notion that the correlation can move the CM in either direction and the action of various aspects of correlation can essentially cancel each other out, as exhibited by the closeness of the DF and fully coupled CM in this case.

Moving further up in Z to Cn ($Z = 112$) a closed $6d$ subshell is now part of the ground state so that the configuration is $[\mathrm{Xe}]4f^{14}5d^{10}5f^{14}6s^26p^66d^{10}7s^2$. The fully coupled $6s \rightarrow \varepsilon p_{3/2}$ CM location is seen from Table II and Fig. 1 to have increased in photoelectron energy to 24.82 a.u., while the two-channel CM has moved to a much higher 29.32 a.u., clearly demonstrating that the interchannel coupling, primarily with a combination of $6d$ and $5f$ photoionization channels, moves the CM to lower energies in this case. The DF CM is at 32.53 a.u. for Cn, which shows that the initial state and intrachannel coupling correlations lower the energy of the CM and interchannel coupling lowers it further. These results again demonstrate that correlations can have significant and complicated effects on the location of the CM.

Now considering the heaviest known element, Og ($Z = 118$), where a $7p$ subshell has been added resulting in a $[\mathrm{Xe}]4f^{14}5d^{10}5f^{14}6s^26p^66d^{10}7s^27p^6$ ground state configuration, a remarkable result is seen: the fully coupled CM has moved to a photoelectron energy of 171.02 a.u. (4653.45 eV), a huge increase over the position in Cn. On the other hand, the two-channel and DF results are increased over Cn to 63.02 a.u. and 62.12 a.u. respectively, but not nearly so dramatic an increase as exhibited by the fully coupled CM. This close agreement between DF and two-channel results indicates that, in this case, initial state and intrachannel coupling correlations are not important (or cancel out). Thus, interchannel coupling must be responsible for the huge increase in the energy of the fully coupled CM. To understand why interchannel coupling affects Og so differently than No and Cn, and why the effects of interchannel coupling are so complicated, we look at the problem from a perturbation theory point of view. The fully coupled dipole matrix element $D_i(E)$ of channel i can be written in terms of the uncoupled matrix elements $M_j(E)$ of the various photoionization channels j as [28]

$$D_i(E) = M_i(E) + \sum_j \int dE' \frac{\langle \psi_i(E)|H - H_0|\psi_j(E')\rangle}{E - E'} M_j(E'), \tag{5}$$

where H–H_0 is the perturbing Hamiltonian, and $\psi_i(E)$ and $\psi_j(E')$ are, respectively, the unperturbed final continuum state wave functions of channels i and j with energies E and E'; the second term on the right of Eq. (5) represents the interchannel coupling contribution to the dipole matrix element. Now, if i represents the $6s \rightarrow \varepsilon p_{3/2}$ channel and the $j's$ are the rest of the photoionization channels, Eq. (5) shows that the interchannel contribution of a given channel j depends upon the magnitude and sign of its dipole matrix element $M_j(E')$, the interchannel coupling matrix element, $\langle \psi_i(E)|H - H_0|\psi_j(E')\rangle$, and whether or not channel j is open (energetically allowed) or closed at the given energy. But most importantly, the influence of the interchannel coupling term is generally largest when the channel j can occur at the same energy as channel i, i.e., they are degenerate so the denominator in Eq. (5) can vanish [29]. And this is exactly what distinguishes the Og case from the lower Z atoms; the interchannel coupling with the $4f$ channels is responsible for the contrasting differences. The $4f$ binding energies for No, Cn, and Og are, respectively, about 24, 38, and 49 a.u., while the corresponding two-channel CM (unperturbed by interchannel coupling) are at 5.70, 29.32, and 63.02 a.u., respectively. In other words, the $4f$ photoionization channels are closed at the energies of the unperturbed CM in No and Cn, but for Og, the unperturbed CM is well above the $4f$ thresholds so the $4f$ channels are open. In addition, since the $4f$ cross sections are more than two orders of magnitude larger than the $6s$ cross section around a photon energy of 60 a.u. and are, in fact, the largest subshell cross sections in this energy range [15], it is clear that the interchannel coupling of the $4f$ channels with $6s$ can alter the $6s$ channels dramatically; that is exactly what is seen.

A side note concerning the $6s \rightarrow \varepsilon p_{3/2}$ channel is that in Og, and only in Og, a second CM is found at a photoelectron energy of 35.02 a.u.; there is no indication of a second CM in this channel for any of the lower Z elements. This is evidently due to a combination of very strong relativistic effects along with correlation in the form of interchannel coupling. Our calculation indicates that the crucial coupling to produce this second CM in Og is with the $4f$ photoionization channels. It is of interest to note that this CM occurs just below the opening of the $4f$ channels in Og.

Turning our attention to the $6s \rightarrow \varepsilon p_{1/2}$ channel, a rather different picture emerges. For Hg, the quasisingle particle results, DF and two-channel RRPA, show a CM quite close to threshold, at photoelectron energies of 0.55 and 0.67 a.u., respectively, as seen in Table II. These tally closely to the nonrelativistic single particle value [9] of 0.23 a.u. and are at significantly lower energy than the $6s \rightarrow \varepsilon p_{3/2}$ channel

TABLE IV. Locus of CM in 5*s* subshells in DF and RRPA.

Atoms	Photoelectron energy (a.u.) of the $5s \rightarrow \varepsilon p_{3/2}$ CM		
	DF	RRPA (two channel)	RRPA (channels coupled according to Table V)
Hg ($Z = 80$)	0.52	0.10	0.40
Rn ($Z = 86$)			
Ra ($Z = 88$)			
No ($Z = 102$)	4.73	1.70	
Cn ($Z = 112$)	19.25	17.46	3.96
Og ($Z = 118$)	45.05	47.10	6.10

CM as also seen from Table II. This is, of course, expected owing to the attractive spin-orbit force in the $6s \rightarrow \varepsilon p_{1/2}$ case. The fully coupled $6s \rightarrow \varepsilon p_{1/2}$ CM in Hg is located at 3.67 a.u., thereby indicating the importance of interchannel coupling in moving the CM to higher energies, just as in the $6s \rightarrow \varepsilon p_{3/2}$ case. However, as expected, the fully coupled CM in Hg is at higher energy for the $6s \rightarrow \varepsilon p_{3/2}$ case.

For all of the higher-Z $6s \rightarrow \varepsilon p_{1/2}$ cases, the DF and two-channel CM lie below threshold, owing to the increasingly attractive spin-orbit force that pulls the $\varepsilon p_{1/2}$ closer to the nucleus. Note parenthetically that the nonrelativistic single particle CM lies just above threshold, 0.02 a.u., for Rn ($Z = 86$) and below threshold for all of the higher Z elements. However, the fully coupled CM lie above threshold for all of the higher-Z cases, as shown in Table II. This indicates that the interchannel coupling pushing the CM to higher energies gets progressively stronger, with increasing Z, so as to overcome the effects of the increasingly attractive spin-orbit force. This is a delicate balance between two large effects in opposite directions and, as a result, no discernible pattern is evident in the locations of the fully coupled $6s \rightarrow \varepsilon p_{1/2}$ CM. However, the splitting in energy between the $6s \rightarrow \varepsilon p_{3/2}$ and the $6s \rightarrow \varepsilon p_{1/2}$ CM, as a function of Z, does follow a very definite pattern; the splitting exhibits a monotone increase, as a function of Z, from 0.50 a.u. for Hg to 1.50 a.u. for Rn, 2.50 a.u. for Ra, 5.00 a.u. for No, 20.00 a.u. for Cn, and finally 167.50 for Og. It is thus clear that the 6*s* CM energy splittings increase dramatically with increasing Z for these heavy atoms.

In the light of the phenomenology seen for the $6s \rightarrow \varepsilon p_{3/2}$ CM it is of interest to look at the photoionization of the 5*s* and 4*s* states to inquire as to whether the combined effects of the relativistic spin-orbit repulsion along with interchannel coupling effects could place the $5s \rightarrow \varepsilon p_{3/2}$ or $4s \rightarrow \varepsilon p_{3/2}$ CM in the continuum for some of the higher Z elements. Note that, due to the strong attractive nature of the spin-orbit forces for the $\varepsilon p_{1/2}$ final continuum wave functions, the CM in the $5s \rightarrow \varepsilon p_{1/2}$ and $4s \rightarrow \varepsilon p_{1/2}$ channels, in the atoms considered, are all in the discrete region.

The results of the present 5*s* calculations are exhibited in Table IV and Fig. 2; for the fully correlated RRPA calculations, the relativistic single excitation channels from subshells listed in Table V are coupled. The CM locations in Table IV are tabulated with respect to the respective 5*s* thresholds of atoms listed in Table I. From Table IV and Fig. 2 it is seen that there appears a $5s \rightarrow \varepsilon p_{3/2}$ CM in Hg just above threshold in the fully coupled RRPA, the two-channel RRPA and the DF calculations. In the case of Rn and Ra, on the other hand, the CM has moved into the discrete in all three levels of calculation. For No, the CM is in the continuum (but pretty close to threshold) in the DF and two-channel RRPA calculations but is still below threshold in the fully coupled RRPA calculation. The clear implication is that the interchannel coupling moves the 5*s* CM to lower energies. For Cn, the spin-orbit repulsion on the $\varepsilon p_{3/2}$ continuum wave function is strong enough that the DF and two-channel RRPA predict the location of $5s \rightarrow \varepsilon p_{3/2}$ CM well into the continuum, at photoelectron energies of 19.25 and 17.46 a.u. respectively. However, interchannel coupling works strongly in the other direction in this case, just as in the case of No, so that the fully coupled RRPA result is predicted to be at 3.96 a.u. photoelectron energy. For Og, the spin-orbit repulsion is even stronger and the DF and two-channel RRPA CM are seen in Table IV and Fig. 2 to locate above 40 a.u. The interchannel coupling moves the CM in the opposite direction and the fully coupled RRPA CM is at 6.10 a.u. photoelectron energy.

There are two noteworthy aspects of these 5*s* results. First is the phenomenon of a CM moving below threshold with increasing Z, as in the nonrelativistic case [9], and subsequently, with further increases in Z, moving back into the continuum owing to relativistic effects. In addition, it is of interest to note that, at the higher $Z's$, the $5s \rightarrow \varepsilon p_{3/2}$ CM is pushed to lower energies by interchannel coupling while in the $6s \rightarrow \varepsilon p_{3/2}$ case the CM is pushed to higher energies by

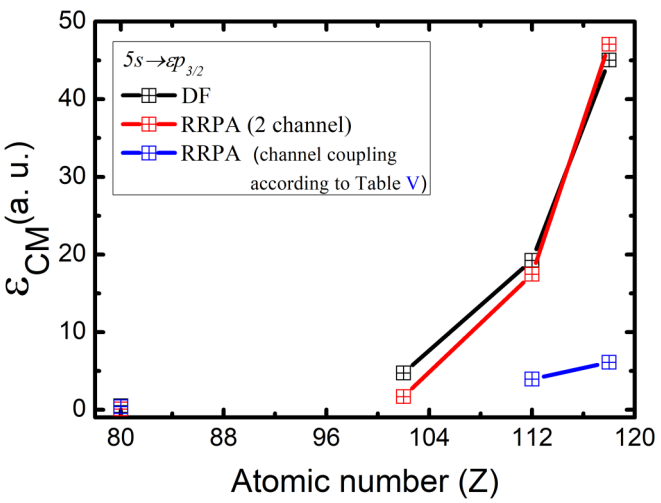

FIG. 2. Locus of 5*s* Cooper minimum locations in photoelectron energy (a. u.) on a linear scale.

TABLE V. Channels coupled for the most correlated (full coupling) RRPA calculations.

Atom	Channels coupled	
Hg ($Z = 80$)	34 channels:	
		$4f_{7/2} \to \varepsilon g_{9/2}, \varepsilon g_{7/2}, \varepsilon d_{5/2}$
	$6s_{1/2} \to \varepsilon p_{3/2}, \varepsilon p_{1/2}$	$4f_{5/2} \to \varepsilon g_{7/2}, \varepsilon d_{5/2}, \varepsilon d_{3/2}$
	$5d_{5/2} \to \varepsilon f_{7/2}, \varepsilon f_{5/2}, \varepsilon p_{3/2}$	$4d_{5/2} \to \varepsilon f_{7/2}, \varepsilon f_{5/2}, \varepsilon p_{3/2}$
	$5d_{3/2} \to \varepsilon f_{5/2}, \varepsilon p_{3/2}, \varepsilon p_{1/2}$	$4d_{3/2} \to \varepsilon f_{5/2}, \varepsilon p_{3/2}, \varepsilon p_{1/2}$
	$5p_{3/2} \to \varepsilon d_{5/2}, \varepsilon d_{3/2}, \varepsilon s_{1/2}$	$4p_{3/2} \to \varepsilon d_{5/2}, \varepsilon d_{3/2}, \varepsilon s_{1/2}$
	$5p_{1/2} \to \varepsilon d_{3/2}, \varepsilon s_{1/2}$	$4p_{1/2} \to \varepsilon d_{3/2}, \varepsilon s_{1/2}$
	$5s_{1/2} \to \varepsilon p_{3/2}, \varepsilon p_{1/2}$	$4s_{1/2} \to \varepsilon p_{3/2}, \varepsilon p_{1/2}$
Rn ($Z = 86$)	39 channels:	
	34 channels listed for Hg+	$6p_{3/2} \to \varepsilon d_{5/2}, \varepsilon d_{3/2}, \varepsilon s_{1/2}$
		$6p_{1/2} \to \varepsilon d_{3/2}, \varepsilon s_{1/2}$
Ra ($Z = 88$)	41 channels:	
	39 channels listed for Rn+	$7s_{1/2} \to \varepsilon p_{3/2}, \varepsilon p_{1/2}$
No ($Z = 102$)	45 channels:	
		$5p_{3/2} \to \varepsilon d_{5/2}, \varepsilon d_{3/2}, \varepsilon s_{1/2}$
	$7s_{1/2} \to \varepsilon p_{3/2}, \varepsilon p_{1/2}$	$5p_{1/2} \to \varepsilon d_{3/2}, \varepsilon s_{1/2}$
	$6p_{3/2} \to \varepsilon d_{5/2}, \varepsilon d_{3/2}, \varepsilon s_{1/2}$	$5s_{1/2} \to \varepsilon p_{3/2}, \varepsilon p_{1/2}$
	$6p_{1/2} \to \varepsilon d_{3/2}, \varepsilon s_{1/2}$	$4f_{7/2} \to \varepsilon g_{9/2}, \varepsilon g_{7/2}, \varepsilon d_{5/2}$
	$6s_{1/2} \to \varepsilon p_{3/2}, \varepsilon p_{1/2}$	$4f_{5/2} \to \varepsilon g_{7/2}, \varepsilon d_{5/2}, \varepsilon d_{3/2}$
	$5f_{7/2} \to \varepsilon g_{9/2}, \varepsilon g_{7/2}, \varepsilon d_{5/2}$	$4d_{5/2} \to \varepsilon f_{7/2}, \varepsilon f_{5/2}, \varepsilon p_{3/2}$
	$5f_{5/2} \to \varepsilon g_{7/2}, \varepsilon d_{5/2}, \varepsilon d_{3/2}$	$4d_{3/2} \to \varepsilon f_{5/2}, \varepsilon p_{3/2}, \varepsilon p_{1/2}$
	$5d_{5/2} \to \varepsilon f_{7/2}, \varepsilon f_{5/2}, \varepsilon p_{3/2}$	$4p_{3/2} \to \varepsilon d_{5/2}, \varepsilon d_{3/2}, \varepsilon s_{1/2}$
	$5d_{3/2} \to \varepsilon f_{5/2}, \varepsilon p_{3/2}, \varepsilon p_{1/2}$	$4p_{1/2} \to \varepsilon d_{3/2}, \varepsilon s_{1/2}$
Cn ($Z = 112$)	49 channels:	
	$6d_{5/2} \to \varepsilon f_{7/2}, \varepsilon f_{5/2}, \varepsilon p_{3/2}$	$5p_{3/2} \to \varepsilon d_{5/2}, \varepsilon d_{3/2}, \varepsilon s_{1/2}$
	$6d_{3/2} \to \varepsilon f_{5/2}, \varepsilon p_{3/2}, \varepsilon p_{1/2}$	$5p_{1/2} \to \varepsilon d_{3/2}, \varepsilon s_{1/2}$
	$6p_{3/2} \to \varepsilon d_{5/2}, \varepsilon d_{3/2}, \varepsilon s_{1/2}$	$5s_{1/2} \to \varepsilon p_{3/2}, \varepsilon p_{1/2}$
	$6p_{1/2} \to \varepsilon d_{3/2}, \varepsilon s_{1/2}$	$4f_{7/2} \to \varepsilon g_{9/2}, \varepsilon g_{7/2}, \varepsilon d_{5/2}$
	$6s_{1/2} \to \varepsilon p_{3/2}, \varepsilon p_{1/2}$	$4f_{5/2} \to \varepsilon g_{7/2}, \varepsilon d_{5/2}, \varepsilon d_{3/2}$
	$5f_{7/2} \to \varepsilon g_{9/2}, \varepsilon g_{7/2}, \varepsilon d_{5/2}$	$4d_{5/2} \to \varepsilon f_{7/2}, \varepsilon f_{5/2}, \varepsilon p_{3/2}$
	$5f_{5/2} \to \varepsilon g_{7/2}, \varepsilon d_{5/2}, \varepsilon d_{3/2}$	$4d_{3/2} \to \varepsilon f_{5/2}, \varepsilon p_{3/2}, \varepsilon p_{1/2}$
	$5d_{5/2} \to \varepsilon f_{7/2}, \varepsilon f_{5/2}, \varepsilon p_{3/2}$	$4p_{3/2} \to \varepsilon d_{5/2}, \varepsilon d_{3/2}, \varepsilon s_{1/2}$
	$5d_{3/2} \to \varepsilon f_{5/2}, \varepsilon p_{3/2}, \varepsilon p_{1/2}$	$4p_{1/2} \to \varepsilon d_{3/2}, \varepsilon s_{1/2}$
Og ($Z = 118$)	56 channels:	
	$7p_{3/2} \to \varepsilon d_{5/2}, \varepsilon d_{3/2}, \varepsilon s_{1/2}$	
	$7p_{1/2} \to \varepsilon d_{3/2}, \varepsilon s_{1/2}$	$5p_{3/2} \to \varepsilon d_{5/2}, \varepsilon d_{3/2}, \varepsilon s_{1/2}$
	$7s_{1/2} \to \varepsilon p_{3/2}, \varepsilon p_{1/2}$	$5p_{1/2} \to \varepsilon d_{3/2}, \varepsilon s_{1/2}$
	$6d_{5/2} \to \varepsilon f_{7/2}, \varepsilon f_{5/2}, \varepsilon p_{3/2}$	$5s_{1/2} \to \varepsilon p_{3/2}, \varepsilon p_{1/2}$
	$6d_{3/2} \to \varepsilon f_{5/2}, \varepsilon p_{3/2}, \varepsilon p_{1/2}$	$4f_{7/2} \to \varepsilon g_{9/2}, \varepsilon g_{7/2}, \varepsilon d_{5/2}$
	$6p_{3/2} \to \varepsilon d_{5/2}, \varepsilon d_{3/2}, \varepsilon s_{1/2}$	$4f_{5/2} \to \varepsilon g_{7/2}, \varepsilon d_{5/2}, \varepsilon d_{3/2}$
	$6p_{1/2} \to \varepsilon d_{3/2}, \varepsilon s_{1/2}$	$4d_{5/2} \to \varepsilon f_{7/2}, \varepsilon f_{5/2}, \varepsilon p_{3/2}$
	$5f_{7/2} \to \varepsilon g_{9/2}, \varepsilon g_{7/2}, \varepsilon d_{5/2}$	$4d_{3/2} \to \varepsilon f_{5/2}, \varepsilon p_{3/2}, \varepsilon p_{1/2}$
	$5f_{5/2} \to \varepsilon g_{7/2}, \varepsilon d_{5/2}, \varepsilon d_{3/2}$	$4p_{3/2} \to \varepsilon d_{5/2}, \varepsilon d_{3/2}, \varepsilon s_{1/2}$
	$5d_{5/2} \to \varepsilon f_{7/2}, \varepsilon f_{5/2}, \varepsilon p_{3/2}$	$4p_{1/2} \to \varepsilon d_{3/2}, \varepsilon s_{1/2}$
	$5d_{3/2} \to \varepsilon f_{5/2}, \varepsilon p_{3/2}, \varepsilon p_{1/2}$	$4s_{1/2} \to \varepsilon p_{3/2}, \varepsilon p_{1/2}$

the interchannel coupling. This is difficult to understand from a physical standpoint. From a mathematical perspective, however, this can be understood from Eq. (5). The interchannel coupling matrix element in the second term of the equation depends upon the initial state wave function and, since the major lobes of the $5s$ and $6s$ wave functions have opposite signs, this translates into opposite signs for the interchannel coupling matrix elements in the two cases, which explains the difference, at least qualitatively.

Finally, the $4s \to \varepsilon p_{3/2}$ channels have been scrutinized and a phenomenon similar to the $5s \to \varepsilon p_{3/2}$ channels occurs there as well. Table VI and Fig. 3 showcase the CM locations of the $4s \to \varepsilon p_{3/2}$ channel and Table VII shows the subshells included in the fully coupled RRPA calculations. The $4s$ situation is quite a bit more extreme than $5s$ since the CM moved below threshold at about $Z = 36$ in the nonrelativistic single-particle calculation [9] and about $Z = 42$ in the corresponding relativistic calculation [12]. However, at $Z = 112$ (Cn) the $4s \to \varepsilon p_{3/2}$ CM re-emerges. As seen in Table VI and Fig. 3, the DF CM is still below threshold while the two-channel RRPA CM is located just above at 0.60 a.u. photoelectron energy. The addition of interchannel coupling

TABLE VI. Positions of CM in 4*s* subshells in RRPA and DF in photoelectron energy (a.u.).

	Photoelectron energy (a.u.) of the $4s \rightarrow \varepsilon p_{3/2}$ CM		
Atom	DF	RRPA (two channel)	RRPA (full coupling as given in Table VII)
Cn ($Z = 112$)		0.60	9.60
Og ($Z = 118$)	8.73	6.10	40.10
Ubn ($Z = 120$)	25.00	17.50	50.50

is seen to make a significant difference moving the CM well above threshold to 9.60 a.u. photoelectron energy. Moving up to Og, the CM moves up in energy correspondingly. The CM appears at 8.73 a.u. at the DF and 6.10 a.u. at the two-channel RRPA levels, and, with the inclusion of interchannel coupling, the CM locates at 40.10 a.u., a large increase in energy as in the Cn case. To look at this phenomenology a bit further, an (as yet) undiscovered atom, Ubn ($Z = 120$) has been considered. The ground state considered is an addition of $8s^2$ to the Og ground state. As seen in Table VI and Fig. 3, the trend continues with DF and two-channel RRPA CM at 25.00 and 17.50 a.u., respectively, and interchannel coupling moving the CM to 50.50 a.u. In any case, it is evident that the $4s \rightarrow \varepsilon p_{3/2}$ re-emerges and continues to increase in photoelectron energy with increasing *Z*. Furthermore, in this case, the interchannel coupling moves the CM to higher energy, like the $6s \rightarrow \varepsilon p_{3/2}$ case and the behavior is just the reverse of $5s \rightarrow \varepsilon p_{3/2}$ case. This is expected based on our understanding of why the 6*s* and 5*s* cases differ since the major lobe of the 4*s* wave function is of the same sign as the 6*s* wave function, but the opposite of the 5*s* wave function.

IV. CONCLUDING REMARKS

The location of the Cooper minima (CM) in the photoionization of *ns* states of high-*Z* atoms has been found to be profoundly affected by both relativistic interactions and correlation in the form of interchannel coupling, configuration interaction in the final continuum states of the photoionization process. As predicted some time ago using relativistic central-field calculations [11,12], the spin-orbit interaction that is attractive for the $\varepsilon p_{1/2}$ final states and repulsive for the $\varepsilon p_{3/2}$ final states has a major effect on the locations of the CM. Furthermore, these differences were seen to engender huge splittings in energy between the CM of the $ns \rightarrow \varepsilon p_{1/2}$ cases and the $ns \rightarrow \varepsilon p_{3/2}$ cases, illustrated, in particular, for the 6*s* initial states in atoms from $Z = 80$ to $Z = 118$. In addition, it was found that the interchannel coupling interactions were crucial and huge for these high-*Z* atoms, albeit rather complex as to in which direction the CM was moved.

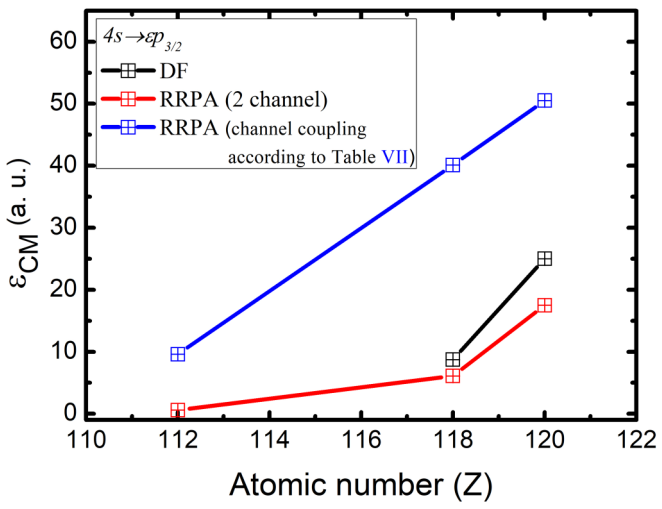

FIG. 3. Locus of 4*s* Cooper minimum locations in photoelectron energy (a. u.) on a linear scale.

For the 6*s* initial state, the spitting in the locations of the CM in $6s \rightarrow \varepsilon p_{3/2}$ and $6s \rightarrow \varepsilon p_{1/2}$ channels was found to increase enormously with increasing *Z*. While at intermediate *Z*′*s* the splitting amounted to a few eV [1], the present results have shown splittings as high as almost 3 keV, thereby illustrating how strongly the relativistic (spin-orbit) force affects the final state wave functions.

Another phenomenon was also uncovered; in certain cases, the $ns \rightarrow \varepsilon p_{3/2}$ CM, that had moved into the discrete region for lower *Z*, re-emerges in the continuum region at high *Z*. This was found for both 5*s* and 4*s* subshells and was also the result of the repulsive spin-orbit force in the final $\varepsilon p_{3/2}$ states of the photoionization process.

As a consequence of the interesting behavior of the CM for *ns* subshells at high *Z*, the angular distribution of the photoelectrons is also similarly affected. If the radial dipole matrix elements for $ns \rightarrow \varepsilon p_{3/2}$ and $ns \rightarrow \varepsilon p_{1/2}$ transitions are the same, then the dipole photoelectron angular distribution parameter β takes on the value 2 and is independent of energy, just like the nonrelativistic prediction [3]. However, if there are differences, which can come about owing to different locations of the CM in the two channels, then β for *ns* photoionization becomes strongly energy dependent [3]. Numerous examples of such behavior have been studied in the past (see, e.g., [19,27,29–31]), but these cases are for situations where the two CM are only separated by a few eV. In the present cases, with such a large splitting of the CM, even in cases when one CM is well above threshold while the other is below threshold, it is likely that a range of different phenomenology in the β parameters will be in evidence. These studies are being pursued and will be reported shortly.

Note further that, although this work deals exclusively with the photoionization of *ns* states, similar phenomenology should appear for the CM of states with nonzero orbital angular momentum for the $l \rightarrow l + 1$ photoionizing transitions where CM exist. Of course, the details will differ for a variety of reasons, including the increased angular momentum barrier "seen" by the higher angular momentum final continuum states. Since the relativistic effects are generated

TABLE VII. Channels coupled for the most correlated (full coupling) RRPA calculations.

Atom	Channels coupled	
Cn ($Z = 112$), Og ($Z = 118$), Ubn ($Z = 120$)	51 channels:	
	$6p_{3/2} \rightarrow \varepsilon d_{5/2}, \varepsilon d_{3/2}, \varepsilon s_{1/2}$	
	$6p_{1/2} \rightarrow \varepsilon d_{3/2}, \varepsilon s_{1/2}$	$4f_{7/2} \rightarrow \varepsilon g_{9/2}, \varepsilon g_{7/2}, \varepsilon d_{5/2}$
	$6s_{1/2} \rightarrow \varepsilon p_{3/2}, \varepsilon p_{1/2}$	$4f_{5/2} \rightarrow \varepsilon g_{7/2}, \varepsilon d_{5/2}, \varepsilon d_{3/2}$
	$5f_{7/2} \rightarrow \varepsilon g_{9/2}, \varepsilon g_{7/2}, \varepsilon d_{5/2}$	$4d_{5/2} \rightarrow \varepsilon f_{7/2}, \varepsilon f_{5/2}, \varepsilon p_{3/2}$
	$5f_{5/2} \rightarrow \varepsilon g_{7/2}, \varepsilon d_{5/2}, \varepsilon d_{3/2}$	$4d_{3/2} \rightarrow \varepsilon f_{5/2}, \varepsilon p_{3/2}, \varepsilon p_{1/2}$
	$5d_{5/2} \rightarrow \varepsilon f_{7/2}, \varepsilon f_{5/2}, \varepsilon p_{3/2}$	$4p_{3/2} \rightarrow \varepsilon d_{5/2}, \varepsilon d_{3/2}, \varepsilon s_{1/2}$
	$5d_{3/2} \rightarrow \varepsilon f_{5/2}, \varepsilon p_{3/2}, \varepsilon p_{1/2}$	$4p_{1/2} \rightarrow \varepsilon d_{3/2}, \varepsilon s_{1/2}$
	$5p_{3/2} \rightarrow \varepsilon d_{5/2}, \varepsilon d_{3/2}, \varepsilon s_{1/2}$	$4s_{1/2} \rightarrow \varepsilon p_{3/2}, \varepsilon p_{1/2}$
	$5p_{1/2} \rightarrow \varepsilon d_{3/2}, \varepsilon s_{1/2}$	$3d_{5/2} \rightarrow \varepsilon f_{7/2}, \varepsilon f_{5/2}, \varepsilon p_{3/2}$
	$5s_{1/2} \rightarrow \varepsilon p_{3/2}, \varepsilon p_{1/2}$	$3d_{3/2} \rightarrow \varepsilon f_{5/2}, \varepsilon p_{3/2}, \varepsilon p_{1/2}$

primarily quite close to the nucleus, the angular momentum barrier likely engenders smaller relativistic effects than in the *ns* photoionization case. However, this should still be of interest and such studies are also being initiated.

ACKNOWLEDGMENT

This work was supported by the U.S. Department of Energy, Office of Science, Basic Energy Sciences under Award No. DE-FG02-03ER15428.

[1] J. W. Cooper, Phys. Rev. **128**, 681 (1962).
[2] J. W. Cooper, Phys. Rev. Lett. **13**, 762 (1964).
[3] S. T. Manson and A. F. Starace, Rev. Mod. Phys. **54**, 389 (1982).
[4] R. W. Ditchburn, Proc. R. Soc. London, Ser. A **117**, 486 (1928).
[5] E. O. Lawrence and N. E. Edelfsen, Phys. Rev. **34**, 1056 (1929).
[6] R. W. Ditchburn, J. Tunstead, and J. G. Yates, Proc. R. Soc. London, Ser. A **181**, 386 (1943).
[7] D. R. Bates, Mon. Not. R. Astron. Soc. **106**, 432 (1946).
[8] D. R. Bates, Proc. R. Soc. London, Ser. A **188**, 350 (1947).
[9] S. T. Manson, Phys. Rev. A **31**, 3698 (1985).
[10] S. Sahoo and Y. H. Ho, Res. Lett. Phys. **2009**, 832413 (2009).
[11] P. C. Deshmukh, B. R. Tambe, and S. T. Manson, Aust. J. Phys. **39**, 679 (1986).
[12] R. Y. Yin and R. H. Pratt, Phys. Rev. A **35**, 1149 (1987).
[13] Y. S. Kim, A. Ron, R. H. Pratt, B. R. Tambe, and S. T. Manson, Phys. Rev. Lett. **46**, 1326 (1981).
[14] P. Jerabek, B. Schuetrumpf, P. Schwerdtfeger, and W. Nazarewicz, Phys. Rev. Lett. **120**, 053001(2018).
[15] A. K. Razavi, R. K. Hosseini, D. A. Keating, P. C. Deshmukh, and S. T. Manson, J. Phys. B **53**, 205203 (2020).
[16] J. Jose, S. Baral, P. C. Deshmukh, and S. T. Manson, Phys. Rev. A **102**, 022813 (2020).
[17] M. Laatiaoui, A. A. Buchachenko, and L. A. Viehland, Phys. Rev. Lett. **125**, 023002 (2020).
[18] M. Reiher and A. Wolf, *Relativistic Quantum Chemistry: The Fundamental Theory of Molecular Science*, 2nd ed. (Wiley-VCH, Wertheim, Germany, 2015).
[19] W. R. Johnson, C. D. Lin, K. T. Cheng, and C. M. Lee, Phys. Scr. **21**, 409 (1980).
[20] W. R. Johnson and C. D. Lin, Phys. Rev. A **20**, 964 (1979).
[21] F. A. Parpia, C. Froese Fischer, and I. P. Grant, Comput. Phys. Commun. **94**. 249 (1996).
[22] F. Salvat, A. Jablonski, and C. J. Powell, Comput. Phys. Commun. **165**, 157 (2005).
[23] E. U. Condon and G. H. Shortley, *The Theory of Atomic Structure* (Cambridge University Press, London, 1951), p. 120ff.
[24] E. W. B. Dias, H. S. Chakraborty, P. C. Deshmukh, S. T. Manson, O. Hemmers, P. Glans, D. L. Hansen, H. Wang, S. B. Whitfield, D. W. Lindle, R. Wehlitz, J. C. Levin, I. A. Sellin, and R. C. C. Perera, Phys. Rev. Lett. **78**, 4553 (1997).
[25] D. L. Hansen, O. Hemmers, H. Wang, D. W. Lindle, P. Focke, I. A. Sellin, C. Heske, H. S. Chakraborty, P. C. Deshmukh, and S. T. Manson, Phys. Rev. A **60**, R2641(R) (1999).
[26] D. J. Kennedy and S. T. Manson, Phys. Rev. A **5**, 227 (1972).
[27] W. R. Johnson and K. T. Cheng, Phys. Rev. A **20**, 978 (1979).
[28] P. C. Deshmukh, V. Radojević, and S. T. Manson, Phys. Lett. **A117**, 293 (1986).
[29] U. Fano, Phys. Rev. **124**, 1866 (1961).
[30] S. B. Whitfield, R. Wehlitz, and V. K. Dolmatov, J. Phys. B **44**, 165002 (2011).
[31] A. Ganesan, S. Deshmukh, G. B. Pradhan, V. Radojević, S. T. Manson, and P. C. Deshmukh, J. Phys. B **46**, 185002 (2013).